PROCEEDINGS OF THE ROYAL SOCIETY A

rspa.royalsocietypublishing.org

Research

Article submitted to journal

Subject Areas:
xxxxx, xxxxx, xxxx

Keywords:
Magneto-rheological elastomers, dimensional reduction, rods, instability, elastica

Author for correspondence:
Insert corresponding author name
e-mail: xxx@xxxx.xx.xx

A nonlinear theory for fibre-reinforced magneto-elastic rods

Jacopo Ciambella[1], Antonino Favata[1] and Giuseppe Tomassetti[2]

[1]Department of Structural and Geotechnical Engineering, Sapienza University of Rome, Italy
[2] Roma Tre University, Engineering Department, Rome, Italy

A model for the finite motion of a magneto-elastic rod reinforced with isotropic (spherical) or anisotropic (ellipsoidal) inclusions is derived from the consistent theoretical framework of 3D variational magneto-elasticity. The particles are assumed weakly and uniformly magnetised, rigid and firmly embedded into the elastomeric matrix. Closed form expression for the quasi-static motion of the rod in terms of the external magnetic field and of the body forces are deduced. Explicit dependences on the shape of the inclusions, their orientation and their anisotropic magnetic properties and the Young modulus of the matrix are deduced. Two case studies are presented, with the rod used as an actuator suspended in a cantilever configuration. This work generalises earlier works from the literature by accounting for both homogeneous and non-homogeneous magnetic field. As such, it can be used as to foster new applications in the field of soft-actuators.

1. Introduction

Magneto-Rheological Elastomers (MREs) are a class of functional materials whose mechanical properties can be controlled upon the application of an external magnetic field by dispersing into a non-magnetic soft matrix, magnetic hard particles. The use of magnetic field to achieve the actuation offers several advantages over other type of actuation such as remote and contactless control as well as the fact that it does not produce any polarization of the media nor chemical alteration [32].

Royal Society Publishing
Informing the science of the future

The magnetization of the reinforcing particles by the external field and the subsequent dipolar interactions give rise to an overall deformation that is amplified by the low elastic modulus of the matrix, usually of the order of 10 MPa or less, and by the high susceptibility of the magnetic particles. This effect is usually referred to as *huge magnetostriction* [28] but must not be confused with the magnetostriction of ferromagnetic crystals as the underlying physical mechanism is completely different[1].

Several type of magnetic particles are nowadays commercially available including *ferromagnetic*, *paramagnetic* or *diamagnetic* fillers [32]. Differences in their atomic nature convey different macroscopic responses: ferromagnetic and paramagnetic particles align parallel to the external magnetic field, whereas diamagnetic particles align perpendicularly; such a different behaviour has been exploited in a number of applications [25,27,41]. Ferromagnetic materials offer the further advantage of susceptibilities several order of magnitude higher than those of paramagnetic or diamagnetic substances and this lowers the magnetic field necessary to achieve the actuation of the samples. This is one of the reason that makes the ferromagnetic carbonyl iron powder one of the most employed filler in MREs [10,30,35,40,41].

Owing to such a large availability of filler types and shapes, MREs provide a much larger design space compared to other type of soft actuators but yet require models able to account for all these features. Upon final cure, the rigid particles are locked in place into the elastomeric matrix, and the composite possess a high degree of flexibility combined with tunable stiffness that makes it capable of bearing large deformations. Moreover, if an external magnetic field is applied during the elastomer cross-linking process, the induced magnetization of the reinforcing particles make them orient along the field lines in a chain-like structure which in turn makes the cured composite transversally isotropic. Therefore, proper models need to be formulated in the framework of large strain transversally isotropic elasticity coupled with magneto-statics.

Some of the existing theoretical studies account for the microgeometry of the composite by evaluating the dipole interactions between adjacent particles assembled in a chain-like structure [22] or randomly dispersed [5]. However, strong kinematics assumptions, i.e., uniaxial deformation in the former, small strains in the latter, are made to obtain closed form expressions of the stress in terms of the magnetic quantities.

The continuum approach to magneto-elastic response of solids dates back to the 50s with the pioneering work of Truesdell, Toupin, Tiersten and Maugin and Eringen (see [13] and references therein). These works used a direct approach to formulate the equilibrium equations based on the conservation laws of continuum mechanics. The same approach was applied by Dorfmann and Ogden [12] to formulate the equilibrium equation of magneto-elasticity at finite strains. Another continuum approach is the one used by Tiersten and Brown [6] (see also [28]), who deduced balance equations by minimizing the potential energy in terms of both magnetic and mechanical quantities; in this approach the equilibrium equations are obtained either as a global minimum or a saddle point of the functional depending upon the choice of the independent magnetic variables (see [15] for a discussion about this point). A judicious choice of the potential energy was used in [20,33] to study the microstructure evolution in transversally isotropic MREs (see also [18]). Kankanala and Triantafyllidis [23] reconciliated the two approaches, direct and variational, by showing that they yield the same governing equations and boundary conditions if the proper independent magnetic variables are chosen.

A variational formulation was more recently used in [16] to derive a micromechanically informed continuum model of MREs that uses a isotropic network model for polymers and extends it to the anisotropic magneto-elastic response. A reduced order model for a MR membrane was introduced in [4] by exploiting the variational approach and assuming uniform and weak magnetization of the reinforcing spherical particles. These assumptions allowed the

[1]In ferromagnetic materials, magnetostriction is caused by the deformation of the crystal lattice whereas in MREs the deformation can either be caused by the particle-particle interactions or by the dipolar interactions with the external magnetic field.

reduction of the integro-differential equations of the general theory, mechanical equilibrium and Maxwell's equations, to a set of differential equations at each material point.

In the past twenty years, a number of experiments has been carried out on MREs. Zrínyi and coworkers have produced and tested several type of magneto-active materials including polymer gels [38,41] and elastomers [39] higlighting phenomena ranging magnetostriction, microscopic instabilities [39] as well as macroscopic instability [38]. Von Lockette et al. [40] produced a silicone elastomer reinforced with spherical rigid and soft magnetic particles and studied the bending behaviour of a specimen suspehended between the platelets of an electromagnets. A similar configuration was exploited by Stanier et al. [37] to study the behaviour of silicone rubber reinforced with nickel coated carbon fibres; different instability mechanisms were highlighted according to the direction of the fibres. The magnetic properties of a MRE (PDMS with carbonyl iron particles) were measured in [10] where two peculiar properties were assessed. First, the magnetisation response appears to be insensitive to the level of prestrain at which the specimen was subjected to. Second, the magnetisation response strongly depends on the relative orientation between the particle chains and the external magnetic field.

Based upon these experimental works, we derive, in the consistent theoretical framework of 3D variational magneto-elasticity, the governing equations for the finite motion of a magneto-elastic rod reinforced with isotropic (spherical) or anisotropic (ellipsoidal) inclusions. The particles are assumed weakly and uniformly magnetised and therefore the potential energy of the system is additively decomposed into a purely mechanical term plus a part accounting for the interaction between the deformation and the external field. The particles are further assumed rigid and firmly embedded into the elastomeric matrix, this in turns makes the demagnetization tensor dependent only on the current orientation of the particles and not on their stretch. It is further introduced an ad-hoc choice of the susceptibility that accounts for both magnetically isotropic or anisotropic materials. These assumptions made possible to derive a closed form expression for the quasi-static motion of the rod in terms of the external magnetic field and of the body forces that act on the beam. This approach generalises the one used in [26,27,37,40] where only a uniform field is considered as well as incorporate the one used in [43] to study the vibration of carbon-nanotubes embedded into a non-uniform magnetic field. It is shown that under certain conditions on the particle distribution and the external field the motion of the beam is governed by the classical elastica equation with forcing terms controlled by the external mangetic field which we call the *magneto-elastica* equation.

The structure of the paper is as follows. In Section 2, we derive the effective magneto-elastic energy of a dilute suspension of magnetic inclusions embedded into an elastic matrix. This expression is used in Section 3 to derive the energy of a rod of such a material by carrying out a formal dimensional reduction. The applications of this theory to two peculiar examples is studied in Section 4, where it is shown that the governing equation of the are reduced to the classical *elastica equation*.

2. The magneto-elastic energy of an assembly of magnetic particles in a non-magnetic elastic matrix

In this Section, following [6] and [23], the variational framework of 3D magneto-elasticity is used to derive an effective magneto-elastic energy of composite reinforced with ellipsoidal inclusions. The following hypotheses are assumed:

(i) the rigid ellipsoidal inclusions are firmly embedded in the non-magnetic soft matrix;
(ii) the inclusions are uniformly magnetized under the external magnetic field;
(iii) the intensity of the field is below the threshold that causes the saturation of the particle magnetisation;
(iv) the suspension of particles is dilute such that magnetic interactions between particles can be neglected.[2]

[2]This is indeed a first order approximation in the volume fraction as shown later in this section.

We start by considering an elastic body reinforced with magnetic inclusions, *e.g.*, a MRE, undergoing a deformation $\boldsymbol{f}:\Omega\to\Omega_c\subset\mathcal{E}$ from its reference configuration Ω to the current configuration Ω_c, a subset of the Euclidean three-dimensional space $\mathcal{E}$. In what follows, we denote by $\boldsymbol{x}$ the current position of the material point $\boldsymbol{X}$ in the reference configuration Ω, that is assumed to be stress free; the deformation gradient $\boldsymbol{F}$ is defined through $\boldsymbol{F}=\mathrm{Grad}\,\boldsymbol{f}:=\partial\boldsymbol{f}/\partial\boldsymbol{X}$. Here and henceforth, we denote by $\mathrm{div}(\cdot)$, $\mathrm{grad}(\cdot)$ and $\mathrm{curl}(\cdot)$ the differential operators with respect to the current coordinates.

In the absence of the elastic body, the problem is governed by the following static Maxwell's equations:

$$\mathrm{div}\boldsymbol{h}_a=0\qquad\text{and}\qquad\mathrm{curl}\,\boldsymbol{h}_a=\boldsymbol{j}_a\qquad\text{in}\quad\mathcal{E},\tag{2.1}$$

where $\boldsymbol{h}_a$ is the field in vacuum and $\boldsymbol{j}_a$ the current density that generates the magnetic field, *e.g.*, the current that flows into an electromagnet.

When the MRE is introduced in the setup and the same currents $\boldsymbol{j}_a$ are switched on, the magnetic field created by these currents will induce a magnetization of the MRE which in turn will generate a *demagnetising field* $\boldsymbol{h}_s$, also known as *stray field*. This field obeys the Maxwell's equations

$$\mathrm{curl}\,\boldsymbol{h}_s=0\quad\text{in}\quad\mathcal{E}\qquad\text{and}\qquad\mathrm{div}\boldsymbol{h}_s=\begin{cases}-\mathrm{div}\boldsymbol{m}, & \text{in}\quad\Omega_c\\ 0, & \text{in}\quad\mathcal{E}\setminus\overline{\Omega_c}\end{cases}\tag{2.2}$$

where $\boldsymbol{m}$ is the *magnetic dipole density* per unit current volume defined inside the body Ω_c, vanishing outside and satisfying the proper jump conditions on the boundary of Ω_c [6]. Therefore, the total magnetic field present during the experiment is $\boldsymbol{h}=\boldsymbol{h}_a+\boldsymbol{h}_s$ and $\boldsymbol{b}=\mu_0(\boldsymbol{h}+\boldsymbol{m})$ is the corresponding magnetic induction field[3].

Under these assumptions, we assume that the energy for the elastic body containing a dilute assembly of non-interacting identical paramagnetic rigid prolate spheroids can be estimated by

$$\mathcal{I}(\boldsymbol{f},\boldsymbol{F},\boldsymbol{a})=\int_\Omega\left\{\Psi_{\mathrm{el}}(\boldsymbol{F},\boldsymbol{a})-\overline{\chi}\frac{\mu_0}{2}\frac{(\boldsymbol{F}\boldsymbol{a}\cdot(\boldsymbol{h}_a\circ\boldsymbol{f}))^2}{|\boldsymbol{F}\boldsymbol{a}|^2}-\widehat{\chi}\frac{\mu_0}{2}(\boldsymbol{h}_a\circ\boldsymbol{f}\cdot\boldsymbol{h}_a\circ\boldsymbol{f})\right\}.\tag{2.3}$$

which is the sum of an elastic energy ψ_{el} accounting for the deformation of the matrix, and two magneto-static terms the former that accounts for the mutual orientation of the particle and the external field, the latter dependent on the field intensity only. In (2.3), the *effective susceptibilities* $\overline{\chi}=\overline{\chi}(\boldsymbol{X})$ and $\widehat{\chi}=\widehat{\chi}(\boldsymbol{X})$ are identified in (2.14) and depend on the volume fraction of magnetic particles at $\boldsymbol{X}$, as well as the magnetic material comprising the particle and on the shape of these particles. In (2.3) $\boldsymbol{a}=\widehat{\boldsymbol{a}}(\boldsymbol{X})$ represents the orientation of the magnetic particle at $\boldsymbol{X}$ in the reference configuration.

In the following part of this Section, we show that (2.3) can be derived as an averaged energy density of an assembly of non-interacting particles.

(a) A variational principle for a single particle

As a first step towards the construction of an averaged energy density, we begin by considering a single homogeneous rigid paramagnetic *prolate spheroid* $\Pi\equiv\Pi(\boldsymbol{a}^c)$ in vacuum, whose major axis in the current configuration is parallel to the unit vector $\boldsymbol{a}^c$, subject to a *spatially–constant* applied magnetic field $\boldsymbol{h}_a$.

If $\boldsymbol{a}^c$ is kept fixed, then the equilibrium magnetization $\boldsymbol{m}$ in the body is a minimizer of the *total magnetostatic energy*

$$\boldsymbol{m}\mapsto\mathcal{M}(\boldsymbol{m},\boldsymbol{a}^c):=\mu_0\int_{\Pi(\boldsymbol{a}^c)}\left\{\frac{1}{2}\boldsymbol{\Upsilon}(\boldsymbol{a}^c)\boldsymbol{m}\cdot\boldsymbol{m}-\boldsymbol{h}_a\cdot\boldsymbol{m}\right\}+\frac{\mu_0}{2}\int_{\mathcal{E}}\boldsymbol{h}\cdot\boldsymbol{h},\tag{2.4}$$

which is the sum of three terms: (i) the Helmholtz-free energy density of the particle, i.e., $\boldsymbol{\Upsilon}(\boldsymbol{a}^c)\boldsymbol{m}\cdot\boldsymbol{m}$, (ii) the interaction energy density between the magnetisation and the external field,

[3]Throughout this paper $\boldsymbol{h}$ and $\boldsymbol{m}$ are assumed to have the same unit of measure, i.e., A/m, whereas the induction field $\boldsymbol{b}$ is in T (see [34] for a discussion on this matter).

also known as *Zeeman energy*, i.e., $\boldsymbol{h}_a \cdot \boldsymbol{m}$, and (iii) the energy density of the magnetic field over the entire space, i.e., $\boldsymbol{h} \cdot \boldsymbol{h}$. By accounting for (2.1)-(2.2), the latter term can be rewritten as

$$\int_{\mathcal{E}} \boldsymbol{h} \cdot \boldsymbol{h} = \int_{\mathcal{E}} \boldsymbol{h}_a \cdot \boldsymbol{h}_a + \int_{\mathcal{E}} \boldsymbol{h}_s \cdot \boldsymbol{h}_s + 2 \int_{\mathcal{E}} \boldsymbol{h}_a \cdot \boldsymbol{h}_s \tag{2.5}$$

in which the integral of $\boldsymbol{h}_a \cdot \boldsymbol{h}_s$ vanishes because the integrand is the product between the divergence-free field $\boldsymbol{h}_a$ and the irrotational field $\boldsymbol{h}_s$ [21] whereas $\int \boldsymbol{h}_a \cdot \boldsymbol{h}_a$ is independent of the state variables and hence can be omitted from the energy calculation (4.22). After simple manipulations, the total magnetostatic energy can be written as

$$\mathcal{M}(\boldsymbol{m}, \boldsymbol{a}^c) = \mu_0 \int_{\Pi(\boldsymbol{a}^c)} \left\{ \frac{1}{2} \boldsymbol{\Upsilon}(\boldsymbol{a}^c) \boldsymbol{m} \cdot \boldsymbol{m} - \left(\frac{1}{2} \boldsymbol{h}_s(\boldsymbol{m}) + \boldsymbol{h}_a \right) \cdot \boldsymbol{m} \right\}, \tag{2.6}$$

in terms of the *inverse susceptibility* tensor $\boldsymbol{\Upsilon}(\boldsymbol{a}^c)$ of the material that comprises the particle and the stray field $\boldsymbol{h}_s(\boldsymbol{m})$ which is determined by $\boldsymbol{m}$ through Maxwell's equations (2.2).

The choice made for the Helmholtz free energy density in (2.6), i.e., quadratic in $\boldsymbol{m}$, implies the magnetisation of the particle to be linear with the external field $\boldsymbol{h}$; this is indeed a reasonable assumption if the particle is made of paramagnetic material or even ferromagnetic material away from the saturation magnetisation [1]. As our notation suggests, we assume that *material and shape symmetries of the particle coincide*, in the sense that $\boldsymbol{\Upsilon}(\boldsymbol{a}^c)$ has one eigenvector parallel to $\boldsymbol{a}^c$ and is a multiple of the identity on the orthogonal complement of $\boldsymbol{a}^c$ [36]:

$$\boldsymbol{\Upsilon}(\boldsymbol{a}^c) = \chi_{\parallel}^{-1} \boldsymbol{a}^c \otimes \boldsymbol{a}^c + \chi_{\perp}^{-1} (\boldsymbol{I} - \boldsymbol{a}^c \otimes \boldsymbol{a}^c). \tag{2.7}$$

The existence and uniqueness of a minimizer of the total magnetostatic energy (4.22) is contingent on the positivity of the inverse suceptibility tensor, which holds true provided that the *susceptibilities* $\chi_{\parallel}$ and $\chi_{\perp}$ are positive. In fact, the positivity of $\boldsymbol{\Upsilon}$ entails that the functional defined in (4.22) is convex and coercive over the space of square–integrable magnetization fields with support in Π. Then, the application of the direct method of the calculus of variations shows that there exists a unique minimizer $\overline{\boldsymbol{m}}$ of the functional $\boldsymbol{m} \mapsto \mathcal{M}(\boldsymbol{m}, \boldsymbol{h}_a, \boldsymbol{a}^c)$. One can also check that $\overline{\boldsymbol{m}}$ is the minimizer if and only if it is a solution of the *Euler–Langrange equation*:

$$\boldsymbol{\Upsilon}(\boldsymbol{a}^c) \overline{\boldsymbol{m}} - \boldsymbol{h}_s(\overline{\boldsymbol{m}}) = \boldsymbol{h}_a \tag{2.8}$$

which holds true because $\boldsymbol{h}_s$ is a linear functional of $\boldsymbol{m}$ (see (2.2)).

(b) The magnetostatic energy as function of its current orientation

Using (2.8) as the characterization of the solution of the minimization problem, one can verify that the minimizer $\overline{\boldsymbol{m}}$ is spatially constant, and also determine it explicitly as a function of the applied field $\boldsymbol{h}_a$. In fact, it is a classical result from magnetostatics [21] that an ellipsoidal body is the only one that can be *uniformly magnetised* under an external homogeneous field. In particular, for the prolate spheroid Π, if $\widetilde{\boldsymbol{m}}$ is the uniform magnetisation, the corresponding demagnetizing field is given by $\boldsymbol{h}_s(\widetilde{\boldsymbol{m}}) = -\boldsymbol{N}(\boldsymbol{a}^c)\widetilde{\boldsymbol{m}}$, where

$$\boldsymbol{N}(\boldsymbol{a}^c) = N_{\parallel} \boldsymbol{a}^c \otimes \boldsymbol{a}^c + N_{\perp} (\boldsymbol{I} - \boldsymbol{a}^c \otimes \boldsymbol{a}^c) \tag{2.9}$$

is the spatial demagnetizing tensor.[4] It is easy to verify that the constant magnetization

$$\overline{\boldsymbol{m}} = (\boldsymbol{\Upsilon}(\boldsymbol{a}^c) + \boldsymbol{N}(\boldsymbol{a}^c))^{-1} \boldsymbol{h}_a \tag{2.10}$$

[4] Explicit formulas are available for the *demagnetizing factors* of a prolate ellipsoid, i.e.,

$$N_{\parallel} = \frac{{a_r}^2}{1 - {a_r}^2} \left[\frac{1}{\sqrt{1 - {a_r}^2}} \operatorname{arcsinh} \left(\frac{\sqrt{1 - {a_r}^2}}{a_r} \right) - 1 \right],$$

$$N_{\perp} = \frac{1}{2} (1 - N_{\parallel}),$$

in terms of the ratio a_r between the axis of symmetry and the transverse axis [21, §3.2.5].

solves (2.8). In fact, since $\overline{\boldsymbol{m}}$ is constant, the associated demagnetizing field is

$$\boldsymbol{h}_s(\overline{\boldsymbol{m}}) = -\boldsymbol{N}(\boldsymbol{a}^c)\overline{\boldsymbol{m}}, \tag{2.11}$$

which together with (2.10) satisfies (2.8).

Having established that (2.10) gives the minimizer, by making use of (2.8) and (2.11), we can introduce a reduced functional that depends on $\boldsymbol{a}^c$ only, viz.

$$\widetilde{\mathcal{M}}(\boldsymbol{a}^c) := \min_{\boldsymbol{m}} \mathcal{M}(\boldsymbol{m}, \boldsymbol{a}^c) = \mathcal{M}(\overline{\boldsymbol{m}}, \boldsymbol{a}^c) = -\frac{\mu_0 V}{2}(\boldsymbol{N}(\boldsymbol{a}^c) + \boldsymbol{\Upsilon}(\boldsymbol{a}^c))^{-1}\boldsymbol{h}_a \cdot \boldsymbol{h}_a, \tag{2.12}$$

where V is the volume of the inclusion Π. By making use of (2.7) and (2.9), we can write

$$\widetilde{\mathcal{M}}(\boldsymbol{h}_a, \boldsymbol{a}^c) = -V\frac{\mu_0}{2}\chi\,(\boldsymbol{a}^c \cdot \boldsymbol{h}_a)^2 - V\frac{\mu_0}{2}\tilde{\chi}|\boldsymbol{h}_a|^2, \tag{2.13}$$

where

$$\chi = (\chi_{\parallel}^{-1} + N_{\parallel})^{-1} - (\chi_{\perp}^{-1} + N_{\perp})^{-1}, \qquad \tilde{\chi} = (\chi_{\perp}^{-1} + N_{\perp})^{-1} \tag{2.14}$$

and V is the volume of Π. This result gives us the dependence of the magnetostatic energy of a single particle as a function of its current orientation $\boldsymbol{a}^c$. Our next step is to derive an expression for the effective energy of a dilute assembly of rigid, identical magnetic particles firmly embedded in an elastic body.

A few remarks. Before proceeding further, a few observations are in order: (i) the expressions of χ and $\tilde{\chi}$ in (2.13) can account for both the magnetic anisotropy and the shape anisotropy of the particle. However, the origin of these two effects are remarkably different: shape anisotropy is caused by the geometry of the particle whereas magnetic anisotropy can be traced back to chemical bonds [1,24]; for example, diamagnetic susceptibilities of the C–C bond are smaller in the direction of the bond ($\chi_{\parallel}$) than that normal to the bond ($\chi_{\perp}$), i.e., $\chi_{\parallel} < \chi_{\perp} < 0$, that is, the anisotropic diamagnetic susceptibility defined by $\chi_a = \chi_{\parallel} - \chi_{\perp}$ is negative. (ii) in the presence of two or more particles, the expression (2.11) for the demagnetizing field should be changed to take into account the demagnetizing field generated by the magnetization distribution outside that particle. However, for d the diameter of a particle, and for D the typical interparticle distance, the intensity of this contribution is of the order of $(d/D)^3$, which is exactly of the same order of magnitude of the volume fraction of magnetic particles. Accordingly, we argue that if the magnetic particles are sufficiently dilute, the mutual interaction between particles can be safely neglected. This is indeed a first order approximation in the volume fraction as shown in [5].

(c) The effective magneto-elastic energy

With the aforementioned remarks in mind, we now consider an elastic body undergoing a deformation $\boldsymbol{f} : \Omega \to \Omega_c \subset \mathcal{E}$ from its reference configuration Ω. For $\boldsymbol{a}$ the *reference orientation* of the magnetic inclusion Π at $\boldsymbol{X}_\Pi \subset \Omega$ in the reference configuration, and for $\boldsymbol{F} \equiv \boldsymbol{F}(\boldsymbol{X}_\Pi) = \nabla \boldsymbol{f}(\boldsymbol{X}_\Pi)$ the deformation gradient at $\boldsymbol{X}_\Pi$, we identify the unit vector

$$\boldsymbol{a}^c = \widehat{\boldsymbol{a}}^c(\boldsymbol{F}, \boldsymbol{a}) = \frac{\boldsymbol{F}\boldsymbol{a}}{|\boldsymbol{F}\boldsymbol{a}|}, \tag{2.15}$$

with the *current orientation* of the particle Π.

Now, to justify our spatial averaging procedure, we make the hypothesis, following [31, §1.4], that it is possible to identify a *mesoscale* ℓ over which statistical quantities, such as volume fraction, are well defined. We assume that over this scale all particles appear as having constant orientation $\boldsymbol{a}$ and the variation of the magnetic field can be neglected at this scale (see Fig. 1).

This assumption allows us to define the *local orientation* $\boldsymbol{a}(\boldsymbol{X})$ and the *local volume fraction* $\nu(\boldsymbol{X})$ as fields in the reference configuration. Neglecting magnetic interaction between particles, we then argue that the magnetostatic energy density per unit referential volume at a typical point

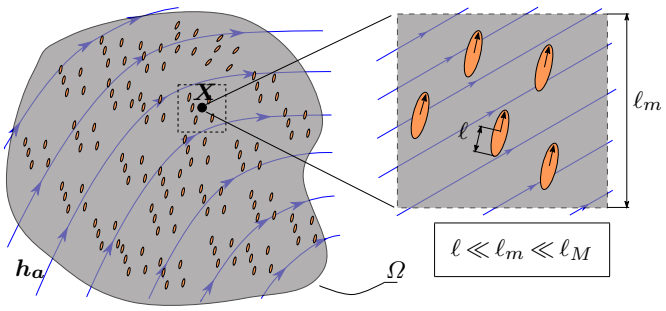

Figure 1. Different homogenisation scales for a magneto-elastic composite reinforced with ellipsoidal inclusions: *macroscale* ℓ_M, i.e., $\ell_M = \int_\Omega \mathrm{d}\Omega$, *mesoscale* ℓ_m, and *characteristic length* of the inclusions ℓ. The variation of the field $\boldsymbol{h}_a$ is assumed negligible at the mesoscale ℓ_m.

$\boldsymbol{X}$ in the reference configuration is equal to the *referential particle density* $\nu(\boldsymbol{X})/V$ multiplied by the magnetostatic energy $\widetilde{M}(\boldsymbol{h}_a, \boldsymbol{a}^c)$ of a single particle with current orientation $\boldsymbol{a}^c(\boldsymbol{F}(\boldsymbol{X}), \boldsymbol{a}(\boldsymbol{X}))$:

$$\psi_{\mathrm{mag}}(\boldsymbol{F}, \boldsymbol{f}, \boldsymbol{a}) = \frac{\nu}{V}\widetilde{M}(\boldsymbol{h}_a \circ \boldsymbol{f}, \widehat{\boldsymbol{a}}^c(\boldsymbol{F}, \boldsymbol{a})). \tag{2.16}$$

The total magnetic energy is obtained by integrating the density ψ_m over Ω; on defining $\overline{\chi} = \nu\chi$ and $\widehat{\chi} = \nu\tilde{\chi}$, and on considering the contribution of the elastic energy of the matrix ψ_{el}, we arrive at (2.3).

Stress and body forces In order to compare our model to the other literature proposals, we now derive the expression of the stress and the body forces induced by the external field $\boldsymbol{h}_a$ by computing the total variation of the total magneto-elastic energy (2.3), i.e.,

$$D\mathcal{I}[\mathring{\boldsymbol{f}}, \mathring{\boldsymbol{F}}] = \int_\Omega \left\{ \frac{\partial \psi_{\mathrm{el}}(\boldsymbol{F})}{\partial \boldsymbol{F}} + \frac{\partial \psi_{\mathrm{mag}}(\boldsymbol{F})}{\partial \boldsymbol{F}} \right\} \cdot \mathring{\boldsymbol{F}} - \int_\Omega \boldsymbol{b}_m \cdot \mathring{\boldsymbol{f}}, \tag{2.17}$$

where, for $\boldsymbol{v}$ a field with unspecified tensorial entity, $\mathring{\boldsymbol{v}}$ denotes its variation. The corresponding *magnetic* Cauchy stress tensor $\boldsymbol{T}_m$, also known as *Maxwell stress*, and the magnetic force per unit *current* volume $\mathfrak{b}_m = J^{-1}\boldsymbol{b}_m$ follows accordingly

$$\boldsymbol{T}_m = J^{-1}\frac{\partial \psi_{\mathrm{mag}}}{\partial \boldsymbol{F}}\boldsymbol{F}^T = \mu_0 J^{-1}\overline{\chi}\left(\boldsymbol{h}_a \cdot \boldsymbol{a}^c\right)\left[\left(\boldsymbol{h}_a \cdot \boldsymbol{a}^c\right)\boldsymbol{a}^c \otimes \boldsymbol{a}^c - \boldsymbol{h}_a \otimes \boldsymbol{a}^c\right], \tag{2.18}$$

$$\mathfrak{b}_m = \mu_0 J^{-1}\overline{\chi}\left(\boldsymbol{h}_a \cdot \boldsymbol{a}^c\right)(\mathrm{grad}\boldsymbol{h}_a)^T\boldsymbol{a}^c + \mu_0 J^{-1}\widehat{\chi}(\mathrm{grad}\boldsymbol{h}_a)^T\boldsymbol{h}_a. \tag{2.19}$$

When the external field is homogeneous, the Maxwell stress (2.18) does not necessarely vanish due to the possible mismatch between the orientation of the magnetic field and the current orientation of the fibres, whereas the body forces $\mathfrak{b}_m$ are zero. This is the main difference between our theory and the others from the literature, e.g., [10,12,23,33], which account for a Maxwell stress only in the presence of non-homogeneous magnetic fields. Indeed, in all those models the Maxwell stress satisfies the differential equations $\mathrm{div}\,\boldsymbol{T}_m = \mu_0(\mathrm{grad}\boldsymbol{h})^T\boldsymbol{m}$, and therefore, when $\boldsymbol{h}$ is homogeneous, only a boundary term is present.

We further remark that the definition (2.18) gives rise to a non symmetric Cauchy stress, in fact

$$\mathrm{skw}\,\boldsymbol{T}_m = -\mu_0 J^{-1}\overline{\chi}\left(\boldsymbol{h}_a \cdot \boldsymbol{a}^c\right)\left(\boldsymbol{h}_a \times \boldsymbol{a}^c\right) \tag{2.20}$$

which represents the body couples that acts on the MRE solid due to the presence of distributed fibres. This expression is formally equivalent to the expression of the torque that acts on an ellipsoidal object embedded into an external magnetic field [8]. When the inclusions are spherical, $\overline{\chi} = 0$ and the corresponding body couples vanishes.

3. Rod-like bodies

If the region occupied by the body Ω is a cylinder with the cross section much smaller than the diameter —what we call a *rod-like body*—, it seems reasonable and convenient to approximate the three-dimensional elastic problem with one-dimensional problems. Specifically, we here are concerned with a functional governing the quasi-static motion of a planar rod modeled as a continuum of planar sections with material curve passing through the center-line of each section. We allow arbitrary bending deformation, we neglect torsion of the rod and we prevent axial extension and shear.

Let us consider a collection of bodies occupying in their undeformed configurations the *rod-like domains* given by $\Omega^{(\varepsilon)} = (0,\ell) \times (-h^{(\varepsilon)}/2, +h^{(\varepsilon)}/2) \times (0,w)$ in a magnetic and mechanical load environment described by the applied magnetic field $\boldsymbol{h}_{\rm a}^{(\varepsilon)}$ and the mechanical loads potential $\mathcal{W}^{(\varepsilon)}(\boldsymbol{\chi})$. To this end, we introduce an orthogonal coordinate system (X,Y,Z) and we let $\{\boldsymbol{c}_1,\boldsymbol{c}_2,\boldsymbol{c}_3\}$ be the associated canonical orthonormal basis. We identify the typical point $\boldsymbol{X}$ with its coordinates, and ε is a small positive parameter. Equilibria for any such body are governed by the energy functional:

$$\widehat{\mathcal{I}}^{(\varepsilon)}(\boldsymbol{f},\boldsymbol{F},\boldsymbol{a}) = \left(\int_{\Omega^{(\varepsilon)}} \psi_{\rm el}(\boldsymbol{F},\boldsymbol{a}) + \psi_{\rm mag}(\boldsymbol{f},\boldsymbol{F},\boldsymbol{a})\right) - \mathcal{W}^{(\varepsilon)}(\boldsymbol{\chi}), \tag{3.1}$$

where we take (2.13) and (2.16) for the magnetic energy.

We are interested in capturing the asymptotic behaviour of the solution of the variational problem (3.1) in the limit as $\varepsilon \to 0$. We work under the following hypotheses:

- thickness and applied magnetic field scale as:

$$h^{(\varepsilon)} = \varepsilon h, \qquad \boldsymbol{h}_{\rm a}^{(\varepsilon)} = \varepsilon \boldsymbol{h}_{\rm a}; \tag{3.2}$$

- the orientation of the magnetic fibers depends only on X:

$$\boldsymbol{a} = \widehat{\boldsymbol{a}}(X). \tag{3.3}$$

Given that we have in mind rod-like bodies, we restrict attention to minimizers of the form

$$\boldsymbol{f}(X,Y) = \boldsymbol{r}(X) + Y\boldsymbol{d}(X), \quad |\boldsymbol{r}'| = 1, \quad \boldsymbol{d} = \boldsymbol{c}_3 \times \boldsymbol{r}' \tag{3.4}$$

The vector $\boldsymbol{r}(X)$ accounts for the deformation of a point X of the *axis* line, while $\boldsymbol{d}(X)$ reckons with the local rotation of a cross section through X. Assumption $(3.4)_2$ implies that the rod is *inextensible*, while $(3.4)_3$ is tantamount to say that the rod is *unshearable*, i.e., the generic cross section maintains orthogonal to the tangent vector to the axis line. It is easily seen that $\boldsymbol{d}' = -\kappa \boldsymbol{r}'$ where $\kappa := \boldsymbol{r}'' \cdot \boldsymbol{d}$ is the *curvature* of the axis, so that the deformation gradient can be recast as

$$\boldsymbol{F}(X,Y) = (1-\kappa Y)\boldsymbol{r}' \otimes \boldsymbol{c}_1 + \boldsymbol{d} \otimes \boldsymbol{c}_2 + \boldsymbol{c}_3 \otimes \boldsymbol{c}_3. \tag{3.5}$$

Here and henceforth $(\cdot)'$ denotes differentiation with respect to X. Since $\{\boldsymbol{r}', \boldsymbol{d}, \boldsymbol{c}_3\}$ is a positively–oriented orthogonal basis, we have that

$$\boldsymbol{F} = \boldsymbol{R}\boldsymbol{U} \qquad \text{with} \qquad \boldsymbol{R} = \boldsymbol{r}' \otimes \boldsymbol{c}_1 + \boldsymbol{d} \otimes \boldsymbol{c}_2 + \boldsymbol{c}_3 \otimes \boldsymbol{c}_3 \qquad \text{and} \qquad \boldsymbol{U} = \boldsymbol{I} - \kappa Y \boldsymbol{c}_1 \otimes \boldsymbol{c}_1 \tag{3.6}$$

is the polar decomposition of the deformation gradient, so that, thanks to the frame indifference of the elastic energy,

$$\int_{\Omega^{(\varepsilon)}} \psi_{\rm el}(\boldsymbol{F},\boldsymbol{a}) = \int_{\Omega^{(\varepsilon)}} \psi_{el}(\boldsymbol{U},\boldsymbol{a}) = w \int_0^{\ell} \int_{-\varepsilon h/2}^{+\varepsilon h/2} \psi_{el}(\boldsymbol{I} - \kappa(X) Y \boldsymbol{c}_1 \otimes \boldsymbol{c}_1, \boldsymbol{a}) \mathrm{d}Y \mathrm{d}X. \tag{3.7}$$

Without loss of generality, we assume that $\psi_{\rm el}(\boldsymbol{I},\boldsymbol{a}) = 0$ and that the reference configuration is stress–free, so that $\partial_{\boldsymbol{F}} \psi_{\rm el}(\boldsymbol{I},\boldsymbol{a}) = \boldsymbol{0}$. Then, performing a Taylor expansion of the integrand with

respect to Y we obtain, in view of the second of (3.6),

$$\psi_{\rm el}(\boldsymbol{I}-\kappa(X)Y\boldsymbol{c}_1\otimes\boldsymbol{c}_1,\boldsymbol{a})=\frac{\kappa^2}{2}\partial^2_{\boldsymbol{FF}}\psi_{\rm el}(\boldsymbol{I},\boldsymbol{a})[\boldsymbol{c}_1\otimes\boldsymbol{c}_1]\cdot(\boldsymbol{c}_1\otimes\boldsymbol{c}_1)Y^2+o(Y^2). \tag{3.8}$$

Since $|Y|<\varepsilon h/2$, we have $o(Y^2)=o(\varepsilon^2)$. Thus, on letting

$$\widetilde{E}(\boldsymbol{a})=\partial^2_{\boldsymbol{FF}}\psi_{\rm el}(\boldsymbol{I},\boldsymbol{a})[\boldsymbol{c}_1\otimes\boldsymbol{c}_1]\cdot\boldsymbol{c}_1\otimes\boldsymbol{c}_1, \tag{3.9}$$

and on substituting (3.8) into (3.7) and on integrating with respect to Y we arrive at

$$\int_{\Omega^{(\varepsilon)}}\psi_{\rm el}(\boldsymbol{Fa})=\frac{1}{2}\int_0^\ell I^{(\varepsilon)}\widetilde{E}(\boldsymbol{a})\kappa^2{\rm d}X+o(\varepsilon^3),\qquad I^{(\varepsilon)}=w\frac{(h^{(\varepsilon)})^3}{12}, \tag{3.10}$$

which is the standard form for the bending energy of a rod made of a transversally isotropic material [2]. In truncating the energy at the third order we are implicitly assuming that the stretching energy of the rod can be neglected compared to the bending and magnetic counterparts.

Next, we turn our attention to the magnetic energy and we made the same third order approximation of the total magnetic energy. Thanks to (3.6), this yields,

$$\begin{aligned}\psi_{\rm mag}(\boldsymbol{F},\boldsymbol{a},\boldsymbol{h}_{\rm a}^{(\varepsilon)})&=-\varepsilon^2\frac{\mu_0}{2}\left\{\overline{\chi}\frac{(\boldsymbol{Ra}\cdot\boldsymbol{h}_a\circ\boldsymbol{f}-\kappa Y(\boldsymbol{c}_1\cdot\boldsymbol{a})(\boldsymbol{Rc}_1\cdot\boldsymbol{h}_a\circ\boldsymbol{f}))^2}{|\boldsymbol{I}-\kappa Y(\boldsymbol{a}\cdot\boldsymbol{c}_1)|^2}+\tilde{\chi}(\boldsymbol{h}_a\circ\boldsymbol{f}\cdot\boldsymbol{h}_a\circ\boldsymbol{f})^2\right\}\\&=-\varepsilon^2\frac{\mu_0}{2}\left\{\overline{\chi}(\boldsymbol{Ra}\cdot\boldsymbol{h}_{\rm a}\circ\boldsymbol{f})^2+\tilde{\chi}(\boldsymbol{h}_a\circ\boldsymbol{f}\cdot\boldsymbol{h}_a\circ\boldsymbol{f})^2\right\}+o(\varepsilon^2).\end{aligned} \tag{3.11}$$

Moreover, we have

$$\boldsymbol{h}_{\rm a}\circ\boldsymbol{f}=\boldsymbol{h}_{\rm a}\circ\boldsymbol{r}+Y(\boldsymbol{h}_{\rm a}\circ\boldsymbol{r})\boldsymbol{d}+o(Y), \tag{3.12}$$

and hence, indeed,

$$\int_{\Omega^{(\varepsilon)}}\psi_{\rm mag}(\boldsymbol{F},\boldsymbol{a},\boldsymbol{h}_{\rm a}^{(\varepsilon)})=-\frac{1}{2}\int_0^\ell\mu_0A^{(\varepsilon)}\left\{\overline{\chi}\,(\boldsymbol{Ra}\cdot\boldsymbol{h}_a^{(\varepsilon)}\circ\boldsymbol{r})^2+\tilde{\chi}\,(\boldsymbol{h}_a^{(\varepsilon)}\circ\boldsymbol{r}\cdot\boldsymbol{h}_a^{(\varepsilon)}\circ\boldsymbol{r})^2\right\}{\rm d}X+o(\varepsilon^3), \tag{3.13}$$

with $A^{(\varepsilon)}=wh^{(\varepsilon)}$.

The total energy of the rod is given by the sum of (3.10) and (3.13). We therefore have

$$\widehat{\mathcal{I}}^{(\varepsilon)}(\boldsymbol{f},\boldsymbol{F},\boldsymbol{a})=\widehat{\mathcal{I}}^{(\varepsilon)}_{1D}(\boldsymbol{r}),\qquad \boldsymbol{r}(X)=\boldsymbol{f}(X,0), \tag{3.14}$$

where

$$\widehat{\mathcal{I}}^{(\varepsilon)}_{1D}(\boldsymbol{r})=\frac{1}{2}\int_0^\ell\left\{I^{(\varepsilon)}\widetilde{E}(\boldsymbol{a})(\boldsymbol{r}')^2-\mu_0\,\overline{\chi}A^{(\varepsilon)}(\boldsymbol{Ra}\cdot\boldsymbol{h}_{\rm a}^{(\varepsilon)}\circ\boldsymbol{r})^2-\mu_0\tilde{\chi}\,(\boldsymbol{h}_a^{(\varepsilon)}\circ\boldsymbol{r}\cdot\boldsymbol{h}_a^{(\varepsilon)}\circ\boldsymbol{r})^2\right\}{\rm d}X. \tag{3.15}$$

It is seen that, apart from the standard elastic contribution, the magnetic energy in (3.15) of the thin rod depends on the mutual orientation of the fibers on the center-line and the external field $\boldsymbol{h}_a$; in this respect, the only part of the deformation gradient that matters is the rotation $\boldsymbol{R}$. It is further seen that, for uniform fields, the latter term in the energy is an additive constant that can be neglected.

Recently, a model of magneto-elastic rods undergoing buckling has been proposed in [19]. Unlike ours, this theory is direct and not deduced from the parent three-dimensional one. In order to derive the governing equations, the authors assume that the local magnetization depends only on the local orientation of the rod with respect to the external field. Moreover, it is postulated that the magnetization orients along the rod axis (if not strictly orthogonal to the field), its longitudinal component is constant and fully determined by the maximum value achieved in the part of the rod that is mostly aligned with the external field, e.g., the free tip of the cantilever rod.

4. Case studies

As an application of the theory developed in previous sections, we derive and solve the governing equation of the cantilever shown in Fig. 2. The rod, subject to a dead vertical load at its free end,

is immersed in a *uniform* magnetic field

$$\boldsymbol{h}_a = H\cos\varphi\,\boldsymbol{c}_1 + H\sin\varphi\,\boldsymbol{c}_2. \tag{4.1}$$

This setup may be regarded as describing a prototypical *robotic arm* which can be used to move the applied load by modulating the external field.

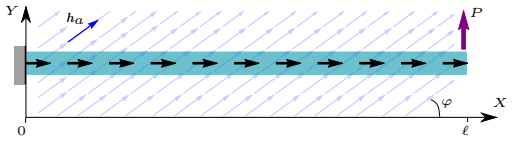

Figure 2. A soft robotic arm in its reference configuration. Dark arrows represent the fibre orientation, i.e., the vector field $\boldsymbol{a}$ in Eq. (4.5), whereas the light blue arrows are indicative of the external field $\boldsymbol{h}_a$ which forms an angle φ with the x-axis.

We introduce the *arclength coordinate* $s = X/\ell \in (0,1)$ and we denote by $\boldsymbol{r}(s)$ the parametric curve that describes the axis of the rod in its typical configuration. Since the rod is inextensible, we can adopt the following representation

$$\boldsymbol{r}'(s) = \cos\vartheta(s)\boldsymbol{c}_1 + \sin\vartheta(s)\boldsymbol{c}_2 \tag{4.2}$$

for the derivative of the curve at the typical point s, and we can express the curve in question as

$$\boldsymbol{r}(s) = (1+u(s))\boldsymbol{c}_1 + v(s)\boldsymbol{c}_2, \tag{4.3}$$

with

$$u(s) = \int_0^s (\cos\vartheta(\bar{s}) - 1)d\bar{s} \quad \text{and} \quad v(s) = \int_0^s \sin\vartheta(\bar{s})d\bar{s}, \tag{4.4}$$

respectively, the horizontal and the vertical displacement.

We assume that in the reference configuration the magnetic fibers are parallel to the X axis, so that the referential and current fiber orientations are, respectively,

$$\boldsymbol{a} = \boldsymbol{c}_1, \qquad \text{and} \qquad \boldsymbol{a}^c(s) = \boldsymbol{r}'(s).$$

We use (3.15) to evaluate the magnetoelastic contribution to the total energy. In doing so, we observe that since the magnetic field is uniform the last term contained in the integral on the right–hand side of (3.15) can be disposed of. We also notice that, by (4.2) we have $|\boldsymbol{r}''|^2 = (\vartheta')^2$; accordingly, for the magnetoelastic energy we can take

$$\widehat{\mathcal{I}}_{\mathrm{ME}}(\vartheta) = \frac{\ell}{2}\int_0^1 \left\{ IE\vartheta'^2 - \mu_0\,\overline{\chi}AH(\cos(\vartheta-\varphi))^2 \right\} \mathrm{d}s \tag{4.5}$$

where $E = \widetilde{E}(\boldsymbol{c}_1)$ is the *effective Young modulus* and we have dropped $^{(\varepsilon)}$ from I and A. It also follows from (4.3) that the load potential is

$$\widehat{\mathcal{I}}_{\mathrm{L}}(\vartheta) = -Pv(1) = -P\int_0^1 \sin\vartheta(s)\mathrm{d}s.$$

The total energy governing equilibria of the cantilever is the sum of the magnetoelastic energy and the load potential. On introducing the dimensionless parameters

$$h^2 = \frac{\mu_0\,\overline{\chi}H^2}{E}\frac{A\ell^2}{I}, \qquad p = \frac{P\ell^2}{EI}, \tag{4.6}$$

we can write $\widehat{\mathcal{I}}_{me}(\vartheta) + \widehat{\mathcal{I}}_p(\vartheta) = \dfrac{EI}{2\ell}\widehat{\mathcal{I}}(\vartheta)$, with

$$\mathcal{I}(\vartheta) = \frac{1}{2}\int_0^1 \left((\vartheta'(s))^2 - h^2(\cos(\vartheta(s)+\varphi))^2 \right) ds - \int_0^1 p\sin\vartheta(s)\,ds. \tag{4.7}$$

We seek configurations $s \mapsto \vartheta(s)$ that render the potential energy $\mathcal{I}$ stationary. Provided that it is twice–continuously differentiable, each such configuration is a solutions of the following boundary–value problem:

$$\begin{cases} \vartheta''(s) - h^2 \sin(2\vartheta(s) + 2\varphi) + p\cos(\vartheta(s)) = 0 \quad \text{for all } s \in (0,1), \\ \vartheta(0) = 0, \\ \vartheta'(1) = 0. \end{cases} \tag{4.8}$$

In the rest of this section we restrict our attention to two cases particularly relevant, the second case having been considered, in a slightly different format, in [37] where experiments have also been conducted.

Case 1. Field aligned with the X-axis ($\varphi = 0$)

The solution of the boundary value problem (4.8) is recovered in closed form only for the two extreme cases, in the absence of the field, i.e., $h = 0$, or in the absence of the load $p = 0$; all intermediate cases must be dealt with numerically. However, a great deal of insight on the underlying mechanics can still be gained by studying separately two regimes, one when the applied load is low, or equivalently the stiffness of the rod is high, i.e., $p \ll 1$ regardless of h, the other one when the applied field is small compared to the load, namely $\xi = h^2/p \ll 1$. We will refer to the former case as *low load regime*, to the latter as *low field regime*.

(a) Low load regime

We firstly examine the case of a low applied load $p \ll 1$, which suggests the following first order perturbation of the solution

$$\vartheta(s) = \vartheta_0(s) + p\,\vartheta_1(s) + o(\delta), \tag{4.9}$$

which leads to the ODE:

$$\vartheta_0'' + p\,\vartheta_1'' - h\,(\sin(2\vartheta_0) + 2\,p\,\vartheta_1\cos(2\vartheta_0)) + p\cos(\vartheta_0) + o(p) = 0, \tag{4.10}$$

where for the sake of conciseness, the dependence on s has been left tacit. By equating the coefficients at the same order, the following cascade of ODEs is obtained:

$$\begin{aligned} &\text{0-th order in } p \qquad \vartheta_0'' - h^2 \sin(2\vartheta_0) = 0 \\ &\text{1-st order } p \qquad \vartheta_1'' - 2h^2\cos(2\vartheta_0)\vartheta_1 = -\cos(\vartheta_0) \end{aligned} \tag{4.11}$$

satisfying the boundary conditions

$$\vartheta_0(0) = \vartheta_0'(1) = 0 \quad \text{and} \quad \vartheta_1(0) = \vartheta_1'(1) = 0, \tag{4.12}$$

respectively.

Notice that $(4.11)_1$ corresponds to the problem of classical elastica, modulo a rescaling of the variable ϑ_0, with a traction load. The unique solution of $(4.11)_1$ is $\vartheta_0(s) = 0$. With this, $(4.11)_2$ reads

$$\vartheta_1'' - 2\,h^2\,\vartheta_1 + 1 = 0, \tag{4.13}$$

endowed with the boundary conditions $(4.12)_2$.

The solution of (4.13) can be easily determined as

$$\vartheta_1(s) = \frac{1}{2\,h^2}\left(1 - \frac{\cosh\left(\sqrt{2}h(s-1)\right)}{\cosh\sqrt{2}h}\right), \tag{4.14}$$

that gives the following vertical displacement of the free end:

$$v_1 := v(s=1) = \int_0^1 \cos(p\,\vartheta_1(s))\mathrm{d}s \simeq p\int_0^1 \vartheta_1(s)\mathrm{d}s = \frac{p}{h^2}\left(\frac{1}{2} - \frac{\sqrt{2}}{4\,h}\tanh(\sqrt{2}h)\right), \tag{4.15}$$

plotted in Fig. 3 for different values of the load p. It is noted that the length of the rod is not constant; this is due to the fact that $|\vartheta| = O(p)$, with $p \ll 1$, while $|u_1 + 1| = o(p)$. In other words, in small rotation approximation, the axial displacement is disregarded.

In this configuration, it is possible to derive the stiffness of the rod in terms of the external magnetic field h. In doing so, we define from (4.15) the map $v_1 \mapsto \widetilde{p}(v_1)$ and, as a consequence, the *stiffness* of the rod is evaluated as

$$\mathfrak{s} := \partial_{v_1}\widetilde{p}(v_1) = \frac{4\,h^3}{2\,h - \sqrt{2}\tanh(\sqrt{2}h)}, \tag{4.16}$$

which is a monotonic increasing function of the external field h; the minimum of the function if achieved when $h \to 0$, for which $\mathfrak{s} \to 3$, that is the stiffness of a cantilever subject to a small vertical load applied at the tip.

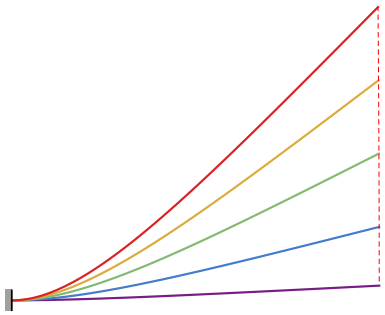

Figure 3. Shape of the rod for increasing $p \in [0, 0.2]$. It is clearly seen that the length of the rod is not constant and this is due to the fact that $|\vartheta| = O(p)$, with $p \ll 1$, while $|u_1 + 1| = o(p)$. **Occhio che se non mettiamo la scala degli assi non si capisce che gli postamenti verticali sono molto più piccoli della lunghezza della trave!**

(b) Low field regime

By defining the smallness parameters $\xi = h^2/p \ll 1$, the solution of (4.8) can be expanded as a power series in ξ as $\vartheta(s) = \vartheta_0(s) + \xi\,\vartheta_1(s) + o(\xi)$. Correspondingly, the following multiscale ODE is obtained

$$\vartheta_0'' + \xi\,\vartheta_1'' - p\,\xi\,(\sin(2\vartheta_0) + 2\,\xi\,\vartheta_1\cos(2\vartheta_0)) + p\,(\cos(\vartheta_0) - \xi\,\vartheta_1\,\sin(\vartheta_0)) + o(\xi) = 0. \tag{4.17}$$

that, by equating the terms at the same order, gives the following cascade of ODEs

$$\text{0-th order in } \xi \qquad \vartheta_0'' + p\cos(\vartheta_0) = 0, \tag{4.18}$$

$$\text{1-st order in } \xi \qquad \vartheta_1'' - p\sin(\vartheta_0)\vartheta_1 = p\sin(\vartheta_0), \tag{4.19}$$

satisfying the boundary conditions[5]

$$\vartheta_0(0) = \vartheta_0'(1) = 0, \qquad \vartheta_1(0) = \vartheta_1'(1) = 0. \tag{4.20}$$

In solving (4.18)-(4.19), we firstly note that the 0-th order Equation (4.18) is the governing equation for the large deflection of a cantilever in absence of the magnetic field. This problem was studied, for instance, in [29,42]. Indeed, qualitative properties of the solutions can be derived from a phase–plane analysis, by recasting the ODE (4.18) into a system of two autonomous first–order differential equations written as:

$$\begin{cases} \vartheta_0' = \kappa_0, \\ \kappa_0' = -p\,\cos\vartheta_0, \end{cases} \tag{4.21}$$

where $\kappa_0 = \vartheta_0'$ is the curvature. Solutions of (4.21) are integral curves of the vector field $\boldsymbol{v} : (\vartheta_0, \kappa_0) \mapsto (\kappa_0, -p\,\cos\vartheta_0)$. Among these solutions, those which originate on the vertical axis, corresponding to $\vartheta_0(0) = 0$, and terminate on the horizontal axis, i.e., $\vartheta_0'(1) = 0$, satisfy the boundary conditions. There are critical values of the load at which multiple solutions start to appear. In particular, the critical points of the vector field $\boldsymbol{v}$ are located on the horizontal axis and can be either *centers* or *saddle points*: all centers form the set $\{(\beta_k, 0) : \beta_k = -\pi/2 + k\pi\}$; all saddle points form the set $\{(\beta_k, 0) : \beta_k = \pi/2 + k\pi\}$. It is also easy to check that the quantity $f(\kappa_0, \vartheta_0) = \kappa_0^2/2 + p\sin\vartheta_0$ is constant along each integral curves. Accordingly, along every such curves, we have:

$$\frac{\kappa_0^2(s)}{2} + p\sin\vartheta_0(s) = p\sin\beta = \frac{\gamma^2}{2}, \qquad \text{where} \quad \beta = \vartheta_0(1) \quad \text{and} \quad \gamma = \kappa_0(0). \tag{4.22}$$

Figure 4 shows the phase diagram and the first four solutions of (4.18), and the corresponding shapes, for $p = 55$ which is higher than the second critical load, i.e., $p_{\text{crit}}^{(2)} \simeq 50.97$[6].

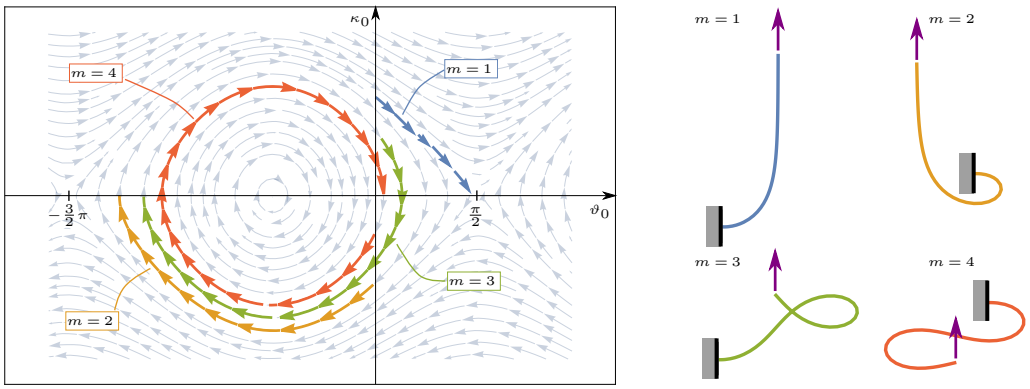

Figure 4. Phase diagram of (4.18) for $p = 55$ with the four solutions and the corresponding mode shapes highlighted.

This multiplicity of solutions is further shown in Fig. 5 where the load p is plotted against the angle $\beta_0 = \vartheta_0(1)$: when $p < p_{\text{crit}}^{(1)} = 10.33$ only one equilibrium solution of (4.18) exists and is represented by the blue branch, i.e., the first deformation mode (point A in the Fig. 5 and $m = 1$ in Fig. 4); when $p > p_{\text{crit}}^{(1)}$, at least other two solutions are found corresponding to shapes B and C ($m = 2$ and $m = 3$ in Fig. 4). It is noted that the transition between the orange and green

[5]Due to the different perturbation parameter used in (4.10) and (4.17), the ϑ_0 and ϑ_1 used in the two equations are, in general, different; however, for the sake of conciseness the same notation is herein used.

[6]For $p > p_{\text{crit}}^{(2)}$ Eq. (4.18) has indeed five solutions but the fifth is not shown in Fig. 4 because either its phase portrait and the shape are similar to the case $m = 4$

branches occurs at $\beta_0 = -\pi$ and $x(1) = 0$, thus the resulting moment at the clamp is zero. It is

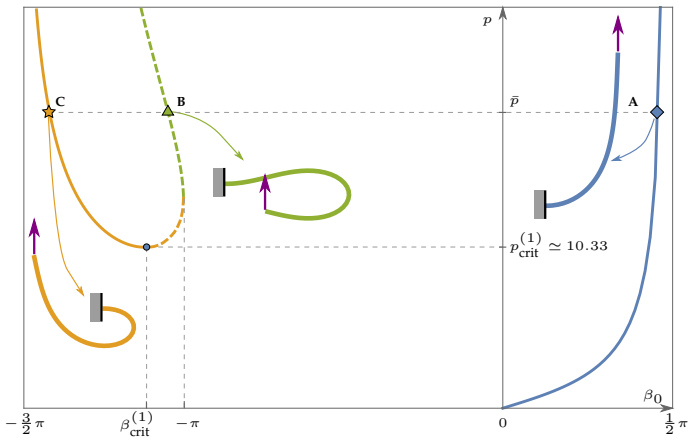

Figure 5. Bifurcation diagram for the 0-th order equation (4.18) for p against $\beta_0 = \vartheta_0(1)$. The first bifurcation occurs when $p = p^{(1)}_{\text{crit}} \simeq 10.33$; further bifurcations are possible at higher loading ($p^{(2)}_{\text{crit}} \simeq 50.97$) but are not shown in the graph. The dashed branch represents unstable equilibria.

further remarked that the set of solutions for $-3\pi/2 < \beta_0 < -\pi$ represented by dashed branch in Fig.5 are unstable equilibria [29] and, consequently, are very difficult to achieve experimentally. On the other hand, the continuous branches are all stable equilibria, although those corresponding to negative β_0, i.e., the orange branch, are at a higher energy content and could be more difficult to observe.

Once the solution of the zero-th order equation ϑ_0 has been obtained, the 1-st order equation (4.19) can be solved numerically. When $p < p^{(1)}_{\text{crit}}$, the solution Eq. (4.18) is unique and so is the solution of (4.19). In fact, the weak version of the homogeneous equation associated to (4.19) is

$$A[\vartheta_1(s), \varphi(s)] := \int_0^1 (\vartheta_1'(s)\varphi'(s) + \gamma(s)\vartheta_1(s)\varphi(s))\mathrm{d}s = 0, \qquad \gamma(s) := p\sin\vartheta_0(s), \tag{4.23}$$

where $\varphi(s) \in C_0^\infty([0,1])$. The bilinear form $A[\vartheta_1(s), \varphi(s)]$ is continuous and, moreover,

$$A[\vartheta_1(s), \vartheta_1(s)] = \int_0^1 \left((\vartheta_1'(s))^2 + \gamma\vartheta_1(s)^2\right)\mathrm{d}s \geq C\|\vartheta_1(s)\|_{H^1([0,1])}, \tag{4.24}$$

which implies $A[\vartheta_1(s), \varphi(s)]$ to be coercive, thence, by the Lax-Milgram theorem, the solution of (4.19) is unique.

Case 2. Field aligned with the Y-axis ($\varphi = \pi/2$)

When the field is perpendicular to the fibres ($\varphi = \pi/2$) and no force is applied ($p = 0$), the governing equation of the problem (4.8) reduces to

$$\vartheta'' + h^2\sin(2\vartheta) = 0, \tag{4.25}$$

with the boundary conditions $\vartheta(0) = 0$ and $\vartheta'(1) = 0$. Equation (4.25) is the classical *elastica*, i.e., the equation that governs the buckling of a column subjected to a compressive loading with $\widehat{\vartheta} = 2\vartheta$ (see [42]); in this sense, the external magnetic field has a *destabilising effect* on the rod.

The qualitative properties of the solutions are better understood by examining the phase portrait of the system

$$\begin{cases} \vartheta' = \kappa, \\ \kappa' = -h^2 \sin(2\,\vartheta), \end{cases} \tag{4.26}$$

which is shown in Fig. 6; it is noted that the symmetry in the phase portrait is due to the invariance of the solutions of (4.26) with respect to the transformation $\tilde{\vartheta} = -\vartheta$. Again, admissible solutions are those which originate on the vertical axis, $\vartheta(0) = 0$, and terminate on the horizontal axis, $\kappa(1) = 0$.

The first integral of (4.25) is

$$\vartheta' = h^2 \left(\cos(2\,\vartheta) - \cos(2\,\beta)\right)$$

that can be integrated in $[0, 1]$ to give the relationship between the applied field and the angle $\beta = \vartheta(1)$, in terms of the following transcendental equation

$$h = \frac{2m-1}{\sqrt{2}}\,\mathrm{ek}(\sin^2(\beta)) \tag{4.27}$$

where ek is the complete elliptic integral of the first kind, i.e., $\mathrm{ek}(q^2) := \int_0^{\pi/2} \left[1 - q^2 \sin^2(\phi)\right]^{-1/2} \mathrm{d}\phi$. Eq. (4.27) has multiple solutions which represent the different modes of deformation and are discriminated by the mode number $m = 1, 2, \ldots$. When $\beta \to 0$, $h_{\mathrm{crit}}^{(m)} = \frac{\pi}{2\sqrt{2}}(2m-1)$ are the critical values of the magnetic field h at which new solutions starts to appear.

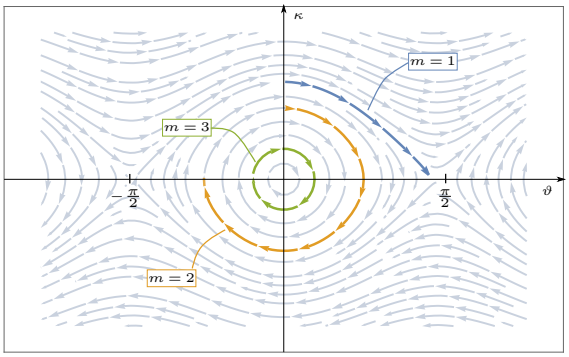

Figure 6. Phase diagram of (4.26) in the plane $\kappa = \vartheta'$ and ϑ, for $h_{\mathrm{crit}}^{(3)} < h < h_{\mathrm{crit}}^{(4)}$ with the first three solution trajectories highlighted.

Equation (4.27) is plotted in Fig. 7 for the first three modes: up to the first critical load $h_{\mathrm{crit}}^{(1)} = \pi/(2\sqrt{2})$ the equation admits only the solution $\vartheta(s) = 0$, i.e., the rod remains straight in its undeformed configuration.

Integration of ((b)) between 0 and $2\vartheta(s)$, $0 < \vartheta(s) < \pi/2$, gives the function $\vartheta(s)$ for the first mode shape, i.e.,

$$\vartheta(s) = \arcsin\left(\sin(\beta)\,\mathrm{sn}(s\sqrt{2}h, \sin^2(\beta))\right) \tag{4.28}$$

which is expressed in terms of the Jacobi elliptic function sn [7]. By using (4.4), the horizontal u_1 and vertical v_1 displacement of the free end ($s = 1$) are obtained by

$$u_1 = \frac{\pi}{2\,\mathrm{ek}(\sin^2(\beta))} - 1 \tag{4.29}$$

$$v_1 = \frac{1}{\mathrm{ek}(\sin^2(\beta))} \log\left(\frac{|\cos(\beta)|}{1 - \sin(\beta)}\right) \tag{4.30}$$

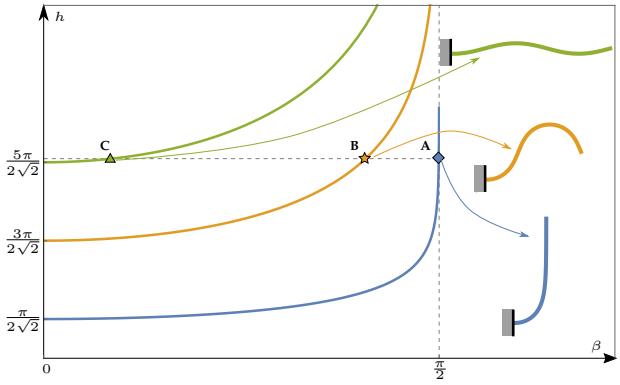

Figure 7. Bifurcation diagram for equation (4.25) for h in terms of $\beta = \vartheta(1)$ given by Eq. (4.27). The three mode shapes are shown for $h_{\text{crit}}^{(3)} < h < h_{\text{crit}}^{(4)}$ and correspond to the paths in the phase portrait shown in Fig. 6. All curves have a vertical asymptote for $\beta \to \pi/2$.

where log is the natural logarithm.

Discussions

The possibility of using the MRE rod in the configuration shown in Fig. 2 as an actuator strongly relies on the capability of controlling its shape by modulating the external field. As such, the appearance of multiple equilibrium configurations could be detrimental unless the transition among them can be accurately controlled or avoided. In this regard, the stability of the actuator, with $\varphi = 0$, is studied in Fig. 8 by looking at the number of solutions in the p, h plane: the green area represents the region in which (4.8) has only one solution, three solutions are found in the orange region, whereas at least five solutions exist in the yellow region. The continuous curves bounding the different regions are the *critical loads*, that is the loads at which new solutions of (4.8) appear. It is noted that in the range $h \in [0, 20]$, the values of $p_{\text{crit}}^{(1)}$ decreases from $p_{\text{crit}}^{(1)} \simeq 10.33$, i.e., is the critical load in the absence of the field, to $p_{\text{crit}}^{(5)} \simeq 5$ for $h = 20$. Such a behaviour highlights the *destabilising* effect that the external field has on the equilibrium of the rod making the second deformation mode appearing at lower loadings; this in turn suggests that, upon the proper control of the external field, the transition between the second to the first mode shape can be used to realise a *magnetic catapult* [3].

On the other hand, if one wanted to use the actuator to lift a weight attached to its tip or move the surrounding fluid in a flap-like configuration, a quasi-static motion with the first mode shape of the configuration with $\varphi = 0$ would be the most effective as it would maximise, for given load and field, the displacement of the free end and at the same time would allow to continuosly control the displacement of the tip by modulating the external field. As a matter of fact, a figure of merit of an actuator is its rigidity in the operative range. For the first mode shape, when the load is low, Eq. (4.16) gives the first order approximation of the rigidity. In the low field regime, the stiffness can be evaluated numerically by solving Eq. (4.19) with ϑ_0 being the first mode shape; for larger fields, the numerical solution of (4.8) can be used. The results of the calculation are plotted for $P = pEI/\ell^2$ against v_1 in Fig. 9 for an actuator with length $\ell = 27.5$ mm, thickness $h = 3$ mm, width $w = 7$ mm, $E = 2.25$ MPa and $\overline{\chi} = 1.32 \times 10^{-4}$, which are the geometric and material properties of the actuator tested in [37] made of PDMS reinforced with 6% vol nickel coated carbon fibres. The dashed lines represents the first order approximation given by Eq. (4.16) whereas the dotted line is the solution for $h = 0$ reported in [29]. By modulating the external field in the range $H \in [0, 5]$ kA/m, the rigidity of the actuator can be changed by two order of magnitude from 4.4×10^{-2}N/m to 1.2 N/m; it is noted that a field value of 10 kA/m can be

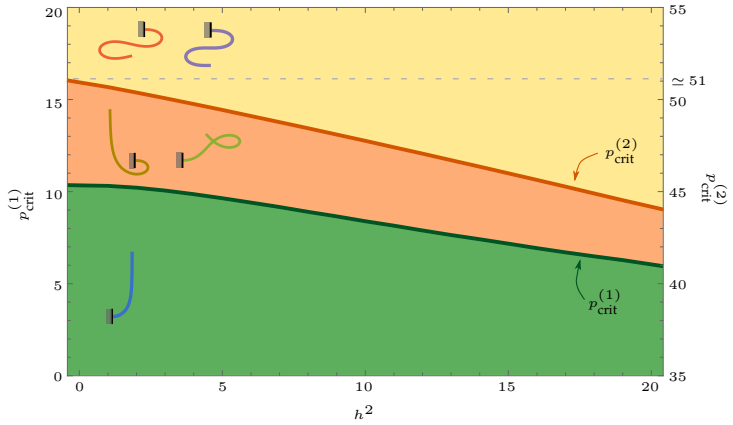

Figure 8. Decrease of the the critical loads $p^{(1)}_{\text{crit}}$ and $p^{(2)}_{\text{crit}}$ of (4.8) with $\varphi = 0$ for an increasing magnetic field in the range $h^2 \in [0, 20]$. The coloured regions represent the number of solutions of the equation: for $p < p^{(1)}_{\text{crit}}$ (gree region) (4.8) has only one solution, for $p^{(1)}_{\text{crit}} < p < p^{(1)}_{\text{crit}}$ (orange region) three solutions, for $p > p^{(3)}_{\text{crit}}$ at least five solutions exist. The corresponding shape of the rod are drawn in the insets.

easily generated by a small neodymium magnet and its below the saturation threshold of the magnetisation of the fibres [37], thus the linear magnetic assumption (2.11) still applies.

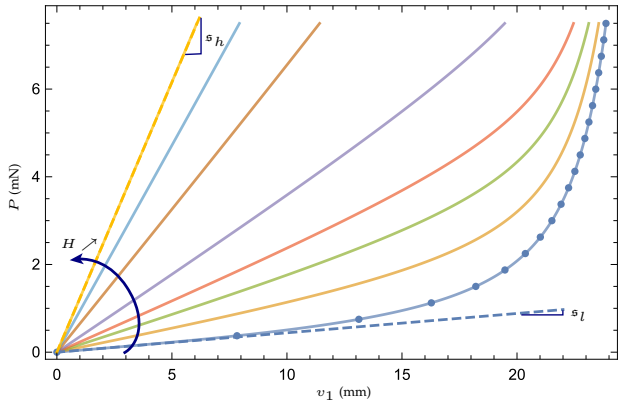

Figure 9. Load, P, against tip vertical displacement, v_1, for the configuration corresponding to mode 1 in Fig. 4. The actuator properties are taken from [37]. The external magnetic field $H \in [0, 5]$ kA/m produces a variation of the actuator rigidity from $\mathfrak{s}_l = 4.4 \times 10^{-2}$ N/m to $\mathfrak{s}_h = 1.2$ N/m. The dashed lines represent the first order approximation (4.16), whereas the dotted line is the solution for $h = 0$ in [29].

The nonlinear model of the rod with $\varphi = \pi/2$ and $p = 0$ is compared to the experimental data from [37] in Fig. 10 in terms of the angle at the free end β and the applied field h. The experimental data shows a sudden increase in the angle in correspondence of a critical value of the field $h^{(1)}_{\text{crit}} \simeq 1.11$. For such a value, the undeformed configuration of the rod $\vartheta(s) = 0$, i.e., the trivial solution of (4.25), becomes unstable and the system releases energy by jumping to the deformed configuration, which, in this case, has the shape of the first mode (insets A, B and C of the figure). This behaviour is due to the interplaying between the elastic bending energy and the

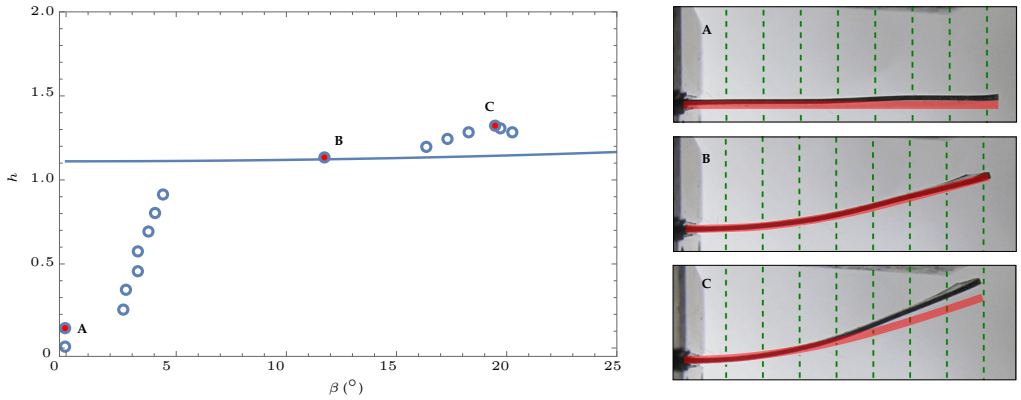

Figure 10. h vs β for the experimental data reported in [37] and the corresponding fitting. The insets show the shape of the actuator for the three different configurations marked as A ($h = 0.12$), B ($h = 1.13$) and C ($h = 1.30$) in the graph. The dashed green lines indicate the direction of the homogeneous magnetic field generated in the experiment by an electromagnet.

magnetic energy in Eq. (4.7): by increasing the external field, the magnetic energy of the system increases and due to the minus sign in (4.7), the undeformed configuration passes from being a minimum of the energy to a maximum, thus the critical transition observed in the figure occurs. The nonlinear model introduced is able to describe this transition as well as the shape of the rod in the post-critical regime.

5. Conclusions and Perspectives

The dispersion of hard magnetic inclusions into a soft matrix is a simple technique to produce soft, remotely controlled actuators that can bear large deformations.

In general the study of such structures requires the simultaneous solution of the equations governing the elastic equilibrium and the Maxwell's equations. However, we have shown that for ellipsoidal and weakly magnetised inclusions dilutely dispersed into an elastic matrix, the equilibrium of the system is governed by a reduced energy functional that depends only on the deformation and in which the magnetic field acts as a source.

Starting from this result, we have derived the governing equations for the quasi-static motion of a rod-like actuator. The model can account for large rotations/displacement of the rod, for the magnetic and shape anisotropy of the inclusions and for homogeneous and non-homogeneous external magnetic fields. As such, it is a generalisation of earlier works [19,27,37].

Two examples have been studied with the actuator suspended in a cantilever configuration. In both cases, under the proper hypothesis, the governing equations have been partially solved in closed form and this has allowed the explicit computations of the shape of the actuator under the different regimes as well as of the critical loads. Different kind of instabilities were highlighted which can be hindered to exploit novel actuator configurations.

The proposed nonlinear model can be extended by accounting for inertial terms that would allow the study large vibrations of slender structures embedded into a magnetic field with applications ranging from MEMS devices to carbon nanotubes.

Acknowledgment

AF acknowledges the financial support of Sapienza University of Rome (Progetto d'Ateneo 2016 – "Multiscale Mechanics of 2D Materials: Modeling and Applications").

References

1. Abbott, J. J., Ergeneman, O., Kummer, M. P., Hirt, A. M., & Nelson, B. J. (2007). *Modeling magnetic torque and force for controlled manipulation of soft-magnetic bodies*. IEEE Transactions on Robotics, 23(6), 1247–1252.
2. Antman, S. S. (2005). Nonlinear problems of elasticity. Springer.
3. Armanini, C., Dal Corso, F., Misseroni, D., & Bigoni, D. (2017). *From the elastica compass to the elastica catapult: an essay on the mechanics of soft robot arm*. Proceedings of the Royal Society A, 473: 20160870.
4. Barham, M., Steigmann, D. J., McElfresh, M., & Rudd, R. E. (2007). *Finite deformation of a pressurized magnetoelastic membrane in a stationary dipole field*. Acta Mechanica, 191(1–2), 1–19.
5. Borcea, L., & Bruno, O. (2001). *On the magneto-elastic properties of elastomer-ferromagnet composites*. Journal of the Mechanics and Physics of Solids, 49(12), 2877–2919.
6. Brown, W. F. (1965). *Theory of magnetoelastic effects in ferromagnetism*. Journal of Applied Physics, 36(3), 994–1000.
7. Byrd, P.F., Friedman, M.D. (1971). *Handbook of Elliptic Integrals for Engineers and Scientists*, Second Edition Springer–Verlag Berlin Heidelberg New Work.
8. Ciambella, J., Stanier, D. C., & Rahatekar, S. S. (2017). *Magnetic alignment of short carbon fibres in curing composites*. Composites Part B: Engineering, 109, 129–137.
9. Ciarlet, P.G. (1997). *Mathematical Elasticity, Vol.II: Theory of Plates*. North Holland, North Holland.
10. Danas, K., Kankanala, S. V, & Triantafyllidis, N. (2012). *Experiments and modeling of iron-particle-filled magnetorheological elastomers*. Journal of the Mechanics and Physics of Solids, 60(1), 120–138.
11. De Simone, A., & Podio-Guidugli, P. (1996). *On the Continuum Theory of Deformable Ferromagnetic Solids*. Archive for Rational Mechanics and Analysis, 136, 201–233.
12. Dorfmann, A., & Ogden, R. W. (2004). *Nonlinear magnetoelastic deformations of elastomers*. Acta Mechanica, 167, 13–28.
13. Dorfmann, L., & Ogden, R. W. (2014). *Nonlinear Theory of Electroelastic and Magnetoelastic Interactions*. Boston, MA: Springer US.
14. Erb, R. M., Martin, J. J., Soheilian, R., Pan, C., & Barber, J. R. (2016). *Actuating Soft Matter with Magnetic Torque*. Advanced Functional Materials, 26(22), 3859–3880.
15. Ericksen, J. L. (2005). *A Modified Theory of Magnetic Effects in Elastic Materials*. Mathematics and Mechanics of Solids, 11(1), 23–47.
16. Ethiraj, G., & Miehe, C. (2016). *Multiplicative magneto-elasticity of magnetosensitive polymers incorporating micromechanically-based network kernels*. International Journal of Engineering Science, 102, 93–119.
17. Galipeau, E., & Ponte Castañeda, P. (2013). *Giant field-induced strains in magnetoactive elastomer composites Giant field-induced strains in magnetoactive elastomer composites*. Proceedings of the Royal Society A, 469, 20130385.
18. Galipeau, E., Rudykh, S., DeBotton, G., & Ponte Castañeda, P. (2014). *Magnetoactive elastomers with periodic and random microstructures*. International Journal of Solids and Structures, 51(18), 3012–3024.
19. Gerbal, F., Wang, Y., Lyonnet, F., Bacri, J.-C., Hocquet, T., Devaud, M. (2015). *A refined theory of magnetoelastic buckling matches experiments with ferromagnetic and superparamagnetic rods*. Proceedings of the National Academy of Sciences of the United States of America, 112(23):7135-7140.
20. Goshkoderia, A., & Rudykh, S. (2017). *Stability of magnetoactive composites with periodic microstructures undergoing finite strains in the presence of a magnetic field*. Composites Part B: Engineering, 128, 19–29.
21. Hubert, A., & Schäfer, R. (1998). *Magnetic Domains: The Analysis of Magnetic Microstructures*. Springer.

22. Jolly, M. R., Carlson, J. D., Munoz, B. C., & Bullions, T. a. (1996). *The magnetoviscoelastic response of elastomer composites consisting of ferrous particles embedded in a polymer matrix*. Journal of Intelligent Material Systems and Structures, 7(6), 613–622.
23. Kankanala, S. V, & Triantafyllidis, N. (2004). *On finitely strained magnetorheological elastomers*. Journal of the Mechanics and Physics of Solids, 52(12), 2869–2908.
24. Kimura, T. (2003). *Study on the Effect of Magnetic Fields on Polymeric Materials and Its Application*. Polymer Journal, 35(11), 823–843.
25. Kimura, T., Yoshino, M., Yamane, T., Yamato, M., & Tobita, M. (2004). *Uniaxial alignment of the smallest diamagnetic susceptibility axis using time-dependent magnetic fields*. Langmuir, 20(14), 5669–5672.
26. Kimura, T., Umehara, Y., & Kimura, F. (2010). *Fabrication of a short carbon fiber/gel composite that responds to a magnetic field*. Carbon, 48(14), 4015–4018.
27. Kimura, T., Umehara, Y., & Kimura, F. (2012). *Magnetic field responsive silicone elastomer loaded with short steel wires having orientation distribution*. Soft Matter, 8(23), 6206–6209.
28. Kovetz, A. (2008). *Electromagnetic Theory*. Oxford Univ Pr.
29. Levyakov, S. V., & Kuznetsov, V. V. (2010). Stability analysis of planar equilibrium configurations of elastic rods subjected to end loads. Acta Mechanica, 211(1–2), 73–87.
30. Li, J., Zhang, M., Wang, L., Li, W., Sheng, P., & Wen, W. (2011). *Design and fabrication of microfluidic mixer from carbonyl iron-PDMS composite membrane*. Microfluidics and Nanofluidics, 10(4), 919–925.
31. Milton, G. W. (2004). The Theory of Composites. (P. G. Ciarlet, Ed.). Cambridge University Press.
32. Rikken, R. S. M., Nolte, R. J. M., Maan, J. C., van Hest, J. C. M., Wilson, D., & Christianen, P. C. M. (2014). *Manipulation of micro- and nanostructure motion with magnetic fields*. Soft Matter, 10(9), 1295–1308.
33. Rudykh, S., & Bertoldi, K. (2013). *Stability of anisotropic magnetorheological elastomers in finite deformations: A micromechanical approach*. Journal of the Mechanics and Physics of Solids, 61(4), 949–967.
34. Scholten, P. C. (1995). *Which SI?*. Journal of Magnetism and Magnetic Materials, 149(1–2), 57–59.
35. Seffen, K. A., & Vidoli, S. (2016). *Eversion of bistable shells under magnetic actuation: a model of nonlinear shapes*. Smart Materials and Structures, 25(6), 065010.
36. Siboni, M. H., & Ponte Castañeda, P. (2012). A magnetically anisotropic, ellipsoidal inclusion subjected to a non-aligned magnetic field in an elastic medium. Comptes Rendus - Mecanique, 340(4–5), 205–218.
37. Stanier, D. C., Ciambella, J., & Rahatekar, S. S. (2016). *Fabrication and characterisation of short fibre reinforced elastomer composites for bending and twisting magnetic actuation*. Composites Part A: Applied Science and Manufacturing, 91, 168–176.
38. Szabo, D., Szeghy, G., & Zrínyi, M. (1998). *Shape transition of magnetic field sensitive polymer gels*. Macromolecules, 31(19), 6541–6548.
39. Varga, Z., Filipcsei, G., & Zrínyi, M. (2006). *Magnetic field sensitive functional elastomers with tuneable elastic modulus*. Polymer, 47(1), 227–233.
40. Von Lockette, P., Lofland, S. E., Biggs, J., Roche, J., Mineroff, J., & Babcock, M. (2011). *Investigating new symmetry classes in magnetorheological elastomers: cantilever bending behavior*. Smart Materials and Structures, 20(10), 105022.
41. Zrínyi, M., Barsi, L., & Buki, A. (1996). *Deformation of ferrogels induced by nonuniform magnetic fields*. The Journal of Chemical Physics, 104(21), 8750–8756.
42. Wang, C. Y. (1981). Large deflections of an inclined cantilever with an end load. International Journal of Non-Linear Mechanics, 16(2), 155–164.
43. Wang, L., Liu, W. B., & Dai, H. L. (2015). *Dynamics and instability of current-carrying microhs in a longitudinal magnetic field*. Physica E: Low-Dimensional Systems and Nanostructures, 66, 87–92.